

MuSiCNet: A Gradual Coarse-to-Fine Framework for Irregularly Sampled Multivariate Time Series Analysis

Jiexi Liu^{1,2}, Meng Cao^{1,2} and Songcan Chen^{1,2}

¹College of Computer Science and Technology, Nanjing University of Aeronautics and Astronautics

²MIIT Key Laboratory of Pattern Analysis and Machine Intelligence

{liujiexi, meng.cao, s.chen}@nuaa.edu.cn

Abstract

Irregularly sampled multivariate time series (ISMTS) are prevalent in reality. Most existing methods treat ISMTS as synchronized regularly sampled time series with missing values, neglecting that the irregularities are primarily attributed to variations in sampling rates. In this paper, we introduce a novel perspective that irregularity is essentially *relative* in some senses. With sampling rates artificially determined from low to high, an irregularly sampled time series can be transformed into a hierarchical set of relatively regular time series from coarse to fine. We observe that additional coarse-grained relatively regular series not only mitigate the irregularly sampled challenges to some extent but also incorporate broad-view temporal information, thereby serving as a valuable asset for representation learning. Therefore, following the philosophy of learning that *Seeing the big picture first, then delving into the details*, we present the **Multi-Scale** and **Multi-Correlation Attention Network** (MuSiCNet) combining multiple scales to iteratively refine the ISMTS representation. Specifically, within each scale, we explore time attention and frequency correlation matrices to aggregate intra- and inter-series information, naturally enhancing the representation quality with richer and more intrinsic details. While across adjacent scales, we employ a representation rectification method containing contrastive learning and reconstruction results adjustment to further improve representation consistency. MuSiCNet is an ISMTS analysis framework that competitive with SOTA in three mainstream tasks consistently, including classification, interpolation, and forecasting.

1 Introduction

Irregularly sampled multivariate time series (ISMTS) are ubiquitous in realistic scenarios, ranging from scientific explorations to societal interactions [Che *et al.*, 2018; Shukla and Marlin, 2021; Sun *et al.*, 2021; Agarwal *et al.*, 2023;

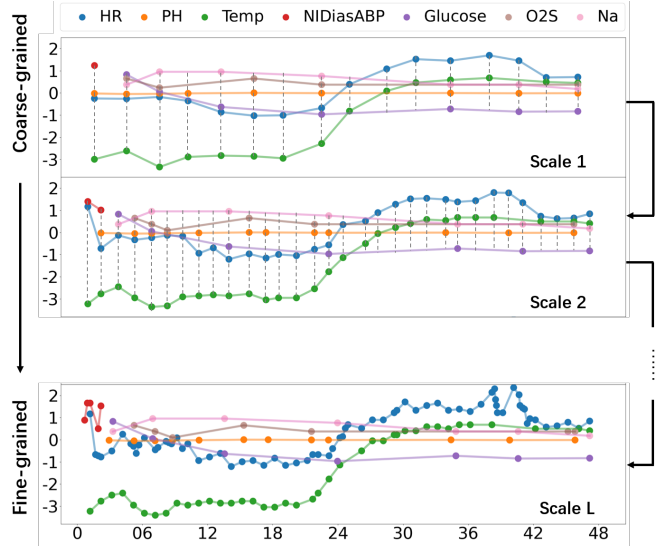


Figure 1: Comparative visualization of multi-scale time series data with various sampling rates. Scale L depicts the original selected representative time series in the P12 Dataset to show the inter- and intra-series irregularities. Scale 1 to Scale $L - 1$ illustrates the effect of applying different sampling rates from low to high.

Yalavarthi *et al.*, 2024]. The causes of irregularities in time series collection are diverse, including sensor malfunctions, transmission distortions, cost-reduction strategies, and various external forces or interventions, etc. Such ISMTS data exhibit distinctive features including intra-series irregularity, characterized by inconsistent intervals between consecutive data points, and inter-series irregularity, marked by a lack of synchronization across multiple variables. The above characteristics typically result in the lack of alignment and uneven count of observations [Shukla and Marlin, 2020], invalidating the assumption of coherent fixed-dimensional feature space for most traditional time series analysis models.

Recent studies have made efforts to address the above problems. Most of them treat the ISMTS as synchronized regularly sampled Normal Multivariate Time Series (NMTS) data with missing values and concentrate on the imputation strategies [Che *et al.*, 2018; Yoon *et al.*, 2018; Camino *et al.*, 2019; Tashiro *et al.*, 2021; Zhang *et al.*, 2021c; Chen *et al.*,

2022; Fan, 2022; Du *et al.*, 2023]. Such direct imputation, however, may distort the underlying relationships and introduce substantial noise, severely compromising the accuracy of the analysis tasks [Zhang *et al.*, 2021b; Wu *et al.*, 2021; Agarwal *et al.*, 2023; Sun *et al.*, 2024]. Latest developments circumvent imputation and aim to address these challenges by embracing the inherent continuity of time, thus preserving the continuous temporal dynamics dependencies within the ISMTS data. Despite these innovations, most methods above are merely solutions for intra-series irregularities, such as Recurrent Neural Networks (RNNs) [De Brouwer *et al.*, 2019; Schirmer *et al.*, 2022; Agarwal *et al.*, 2023]- and Neural Ordinary Differential Equations (Neural ODEs) [Kidger *et al.*, 2020; Rubanova *et al.*, 2019; Jhin *et al.*, 2022; Jin *et al.*, 2022]-based methods and the unaligned challenges presented by inter-series irregularities in multivariate time series remain unsolved.

Delving into the nature of irregularly sampled time series, we discover that the intra- and inter-series irregularities in ISMTS primarily arise from inconsistency in sampling rates within and across variables. We argue that irregularities are essentially relative in some senses and by artificially determined sampling rates from low to high, ISMTS can be transformed into a hierarchical set of relatively regular time series from coarse to fine. Taking a broader perspective, setting a lower and consistent sampling rate within an instance can synchronize sampling times across series and establish uniform time intervals within series. This approach can mitigate both types of irregularity to some extent and emphasize long-term dependencies. As shown in Fig.1, the coarse-grained scales 1 and 2 exhibit balanced placements for all variables in the instance and provide clearer overall trends. However, lower sampling rates may lead to information loss and sacrifice detailed temporal variations. Conversely, with a higher sampling rate as in scale L , more real observations contain rich information and prevent artificially introduced dependencies beyond original relations during training. Nonetheless, the significant irregularity in fine-grained scales poses a greater challenge for representation learning.

To bridge this gap, we propose MuSiCNet—a Multi-Scale and Multi-Correlation Attention Network—to iteratively optimize ISMTS representations from coarse to fine. Our approach begins by establishing a hierarchical set of coarse- to fine-grained series with sampling rates from low to high. **At each scale**, we employ a custom-designed encoder-decoder framework called multi-correlation attention network (CorrNet), for representation learning. The CorrNet encoder (CorrE) captures embeddings of continuous time values by employing an attention mechanism and correlation matrices to aggregate intra- and inter-series information. Since more attention should be paid to correlated variables for a given query which can provide more valuable knowledge, we further design frequency correlation matrices using Lomb–Scargle Periodogram-based Dynamic Time Warping (LSP-DTW) to mitigate the awkwardness in correlation calculation in ISMTS and re-weighting the inter-series attention score. **Across scales**, we employ a representation rectification operation from coarse to fine to iteratively refine the learned representations with contrastive learning and recon-

struction results adjustment methods. This ensures accurate and consistent representation and minimizes error propagation throughout the model.

Benefiting from the aforementioned designs, MuSiCNet explicitly learns multi-scale information, enabling good performance on widely used ISMTS datasets, thereby demonstrating its ability to capture relevant features for ISMTS analysis. Our main contributions can be summarized as follows:

- We find that irregularities in ISMTS are essentially relative in some senses and multi-scale learning helps balance coarse- and fine-grained information in ISMTS representation learning.
- We introduce CorrNet, an encoder-decoder framework designed to learn fixed-length representations for ISMTS. Notably, our proposed LSP-DTW can mitigate spurious correlations induced by irregularities in the frequency domain and effectively re-weight attention across sequences.
- We are not limited to a specific analysis task and attempt to propose a task-general model for ISMTS analysis, including classification, interpolation, and forecasting.

2 Related Work

2.1 Irregularly Sampled Multivariate Time Series Analysis

An effective approach for analyzing ISMTS hinges on the understanding of their unique properties. Most existing methods treat ISMTS as NMTS with missing values, such as [Che *et al.*, 2018; Yoon *et al.*, 2018; Camino *et al.*, 2019; Tashiro *et al.*, 2021; Chen *et al.*, 2022; Fan, 2022; Du *et al.*, 2023; Wang *et al.*, 2024]. However, most imputation-based methods may distort the underlying relationships, introducing unsuitable inductive biases and substantial noise due to incorrect imputation [Zhang *et al.*, 2021b; Wu *et al.*, 2021; Agarwal *et al.*, 2023], ultimately compromising the accuracy of downstream tasks. Some other methods treat ISMTS as time series with discrete timestamps, aggregating all sample points of a single variable to extract a unified feature for each variable [Zhang *et al.*, 2021b; Horn *et al.*, 2020; Li *et al.*, 2023]. These methods can directly accept raw ISMTS data as input but often struggle to handle the underlying relationships within the time series. Recent progress seeks to overcome these challenges by recognizing and utilizing the inherent continuity of time, thereby maintaining the ongoing temporal dynamics present in ISMTS data [De Brouwer *et al.*, 2019; Rubanova *et al.*, 2019; Kidger *et al.*, 2020; Schirmer *et al.*, 2022; Jhin *et al.*, 2022; Chowdhury *et al.*, 2023].

Despite these advancements, existing methods mainly suffer from two main drawbacks, they primarily address intra-series irregularity while overlooking the alignment issues stemming from inter-series irregularity, and 2) they rely on assumptions tailored to specific downstream tasks, hindering their ability to consistently perform well across various ISMTS tasks.

able cannot be uniform for a given query and similar variables that provide more valuable information should receive more attention. Therefore, we designed frequency correlation matrices to re-weight the inter-series attention scores, enhancing the representation learning process.

In general, as illustrated in Fig.2(b), taking ISMTS \mathbf{X} as input, the CorrNet Encoder $\text{CorrE}(\cdot)$ generates multi-time attention embedding as follows:

$$\begin{aligned} \text{CorrE}(\mathbf{Q}_T, \mathbf{K}_T, \mathbf{X}) &= \mathbf{A}_T \mathbf{X} \mathbf{C}_T \\ \mathbf{A}_T &= \text{softmax}(\mathbf{Q}_T \mathbf{K}_T / d_r) \end{aligned} \quad (1)$$

where the calculation of \mathbf{A}_T is based on a time attention mechanism with query \mathbf{Q}_T and key \mathbf{K}_T . Since more attention should be paid to correlated variables for a given query which can provide more valuable knowledge. Therefore, different input dimensions should utilize various weights of time embeddings through the correlation matrix \mathbf{C}_T , and we will introduce it in the next paragraph.

Since the continuous function defined by the CorrE module is incompatible with neural network architectures designed for fixed-dimensional vectors or discrete sequences, following the method in [Shukla and Marlin, 2021], we generate an output representation by materializing its output at a pre-defined set of reference time points $\tau = [\tau_1, \dots, \tau_k]$. This process transforms the continuous output into a fixed-dimensional vector or a discrete sequence, thereby making it suitable for subsequent neural network processing.

Correlation Extraction. The correlation matrix is essential for deriving reliable and consistent correlations within ISMTS, which must be robust to the inherent challenges of variable sampling rates and inconsistent observation counts at each timestamp in ISMTS. Most existing distance measures, such as Euclidean distance, Dynamic Time Warping (DTW) [Berndt and Clifford, 1994], and Optimal Transport/Wasserstein Distance [Villani and others, 2009], risk generating spurious correlations in the context of irregularly sampled time series. This is due to their dependence on the presence of both data points for the similarity measurement, and the potential for imputation to introduce unreliable information before calculating similarity and we will further discuss it in Section 4.5 of our experiments.

At an impasse, the Lomb-Scargle Periodogram (LSP) [Lomb, 1976; Scargle, 1982] provides enlightenment to address this issue. LSP is a well-known algorithm to generate a power spectrum and detect the periodic component in irregularly sampled time series. It extends the *Fourier periodogram* approach to accommodate irregularly sampled scenarios [VanderPlas, 2018] eliminating the need for interpolation or imputation. This makes LSP a great tool for simplifying ISMTS analysis. Compared to existing methods, measuring the similarity between discrete raw observations, LSP-DTW, an implicit continuous method, utilizes inherent periodic characteristics and provides global information to measure the similarity.

As demonstrated in Fig.2(b), we first convert ISMTS into the frequency domain using LSP and then apply DTW to evaluate the distance between variables. The correlation between

\mathbf{X}_{d_i} and \mathbf{X}_{d_j} is:

$$\begin{aligned} c_{d_i d_j} &= \text{DTW}(\text{LSP}(\mathbf{X}_{d_i}), \text{LSP}(\mathbf{X}_{d_j})) \\ &= \min_{\pi} \sum_{(m,n) \in \pi} (\text{LSP}(\mathbf{X}_{d_i})[m] - \text{LSP}(\mathbf{X}_{d_j})[n])^2 \end{aligned} \quad (2)$$

where π is the search path of DTW. We calculate the correlation matrix \mathbf{C}_T by iteratively performing the aforementioned step for an instance.

Encoder-Decoder Framework. Drawing inspiration from notable advances in NLP and CV, our core network, CorrNet employs time series masked modeling, which learns effective time series representations to facilitate various downstream analysis tasks. It is a framework consisting of an encoder-decoder architecture based on continuous-time interpolation. At each scale l , CorrE learns a set of latent representations $\mathbf{r}^{(l)} = [r_1, \dots, r_K]$ defined at K reference time points on the randomly masked ISMTS. We further employ CorrNet Decoder (CorrD), a simplified CorrE (without correlation matrix), to produce the reconstructed output $\hat{\mathbf{X}}_{\text{reco}}^{(l)}$, using the input time point sequence $\mathbf{t}^{(l)}$ as reference points. We iteratively apply the same CorrNet at each scale. Here, we emphasize that all scales share a single encoder that can reduce the model complexity and keep feature extraction consistency for various scales.

We measure the reconstruction accuracy using the Mean Squared Error (MSE) between the reconstructed values and the original ones at each timestamp and calculate the MSE loss specifically for the masked timestamps, as expressed in the following equation

$$\ell_{\text{recon}}^{(l)} = \sum_i \|\mathbf{M}^{(l)} \odot ((\hat{\mathbf{X}}_{\text{reco}}^{(l)})_i - \mathbf{X}_i^{(l)})\|_2^2 \quad (3)$$

where $\mathbf{M}^{(l)}$ is the l -th scale mask, \odot is Hadamard product.

3.3 Rectification Strategy Across Scales

Following the principle that adjacent scales exhibit similar representations and coarse-grained scales contain more long-term information, the rectification strategy is a key component of our MuSiCNet framework. We implement a dual rectification strategy across adjacent scales to enhance representation learning. We start by generating a hierarchical set of relatively regular time series from coarse to fine by

$$\mathbf{X}_{\text{multi}} = \mathbf{M}^{(l)} \odot (\text{AvgPooling}_L(\mathbf{X})) = \{\mathbf{X}_{\text{mask}}^{(1)}, \dots, \mathbf{X}_{\text{mask}}^{(L)}\} \quad (4)$$

While the coarse-grained series ignores detailed variations for high-frequency signals and focuses on much clearer broad-view temporal information, the fine-grained series retains detailed variations for frequently sampled series. As a result, iteratively using coarse-grained information for fine-grained series as a strong structural prior can benefit ISMTS learning.

Firstly, the reconstruction results at scale l is designed to align closely with the results at the $(l-1)$ -th scale, that is to say, the reconstruction results at scale $(l-1)$ can be used to adjust the results at scale l using MSE,

$$\ell_{\text{adj}}^{(l)} = \sum_i \left\| \left((\text{AvgPooling}_l(\hat{\mathbf{X}}_{\text{reco}}^{(l)}))_i - (\hat{\mathbf{X}}_{\text{reco}}^{(l-1)})_i \right) \right\|_2^2 \quad (5)$$

Secondly, contrastive learning is leveraged to ensure coherence between adjacent scales. Pulling these two representations between adjacent scales together and pushing other representations within the batch \mathcal{B} apart, not only facilitates the learning of within-scale representations but also enhances the consistency of cross-scale representations. Taking into consideration that the dimensions of $\mathbf{r}^{(l)}$ and $\mathbf{r}^{(l-1)}$ are different, we employ a GRU Network as a decoder to uniform dimension as $\mathbf{h}^{(l)}$ and $\mathbf{h}^{(l-1)}$ before contrastive learning.

$$\ell_{\text{cons}}^{(l)} = - \sum_i \log \frac{\exp(\mathbf{h}_i^{(l)} \cdot \mathbf{h}_i^{(l-1)})}{\sum_{j=1}^{\mathcal{B}} (\exp(\mathbf{h}_i^{(l)} \cdot \mathbf{h}_j^{(l-1)}) + \mathbb{I}_{[i \neq j]} \exp(\mathbf{h}_i^{(l)} \cdot \mathbf{h}_j^{(l)}))} \quad (6)$$

where the \mathbb{I} is the indicator function. The advantage of the two operations lies in their ability to ensure a consistent and accurate representation of the data at different scales. This strategy significantly improves the model’s ability to learn representations from ISMTS data, which is essential for tasks requiring detailed and accurate time series analysis. Last but not least, this method ensures that the model remains robust and effective even when dealing with data at varying scales, making it versatile for diverse applications.

4 Experiment

In this section, we demonstrate the effectiveness of MuSiCNet framework for time series classification, interpolation and forecasting. *Notably, for each dataset, the window size is initially set to 1/4 of the time series length and then halved iteratively until the majority of the windows contain at least one observation.* Our results are based on the mean and standard deviation values computed over 5 independent runs. **Bold** indicates the best performer, while underline represents the second best. Due to the page limitation, we provide more detailed setup for experiments in the Appendix.

4.1 Time Series Classification

Datasets and experimental settings. We use real-world datasets including healthcare and human activity for classification. (1) **P19** [Reyna *et al.*, 2020] with missing ratio up to 94.9%, includes 38,803 patients that are monitored by 34 sensors. (2) **P12** [Goldberger *et al.*, 2000] records temporal measurements of 36 sensors of 11,988 patients in the first 48-hour stay in ICU, with a missing ratio of 88.4%. (3) **PAM** [Reiss and Stricker, 2012] contains 5,333 segments from 8 activities of daily living that are measured by 17 sensors and the missing ratio is 60.0%. *Importantly, P19 and P12 are imbalanced binary label datasets.*

Here, we follow the common setup by randomly splitting the dataset into training (80%), validation (10%), and test (10%) sets and the indices of these splits are fixed across all methods. Consistent with prior researches, we evaluate the performance of our framework on classification tasks using the area under the receiver operating characteristic curve (AUROC) and the area under the precision-recall curve (AUPRC) for the P12 and P19 datasets, given their imbalanced nature. For the nearly balanced PAM dataset, we employ Accuracy, Precision, Recall, and F1 Score. For all of the above metrics, higher results indicate better performance.

Main Results of classification. We compare MuSiCNet with ten state-of-the-art irregularly sampled time series classification methods, including Transformer [Vaswani *et al.*, 2017], Trans-mean, GRU-D [Che *et al.*, 2018], SeFT [Horn *et al.*, 2020], and mTAND [Shukla and Marlin, 2021], IPNet [Shukla and Marlin, 2018], DGM²-O [Wu *et al.*, 2021], MTGNN [Wu *et al.*, 2020], Raindrop [Zhang *et al.*, 2021b] and ViTST [Li *et al.*, 2023]. Since mTAND is proven superior over various recurrent models, such as RNNImpute [Che *et al.*, 2018], Phased-LSTM [Neil *et al.*, 2016] and ODE-based models like LATENT-ODE and ODE-RNN [Chen *et al.*, 2018], we focus our comparisons on mTAND and do not include results for the latter model.

As indicated in Table 1, MuSiCNet demonstrates good performance across three benchmark datasets, underscoring its effectiveness in typical time series classification tasks. Notably, in binary classification scenarios, MuSiCNet surpasses the best-performing baselines on the P12 dataset by an average of 1.0% in AUROC and 3.0% in AUPRC. For the P19 dataset, while our performance is competitive, MuSiCNet stands out due to its lower time and space complexity compared to ViTST. ViTST converts 1D time series into 2D images, potentially leading to significant space inefficiencies due to the introduction of extensive blank areas, especially problematic in ISMTS. In the more complex task of 8-class classification on the PAM dataset, MuSiCNet surpasses current methodologies, achieving a 0.5% improvement in accuracy and a 0.7% increase in precision.

Notably, the *consistently low standard deviation* in our results indicates that MuSiCNet is a reliable model. Its performance remains steady across varying data samples and initial conditions, suggesting a strong potential for generalizing well to new, unseen data. This stability and predictability in performance enhance the confidence in the model’s predictions, which is particularly crucial in sensitive areas such as medical diagnosis in clinical settings.

4.2 Time Series Interpolation

Datasets and experimental settings. PhysioNet [Silva *et al.*, 2012] consists of 37 variables extracted from the first 48 hours after admission to the ICU. We use all 8,000 instances for interpolation experiments whose missing ratio is 78.0%.

We randomly split the dataset into a training set, encompassing 80% of the instances, and a test set, comprising the remaining 20% of instances. Additionally, 20% of the training data is reserved for validation purposes. The performance evaluation is conducted using MSE, where lower values indicate better performance.

Main Results of Interpolation. For the interpolation task, we compare it with RNN-VAE, L-ODE-RNN [Chen *et al.*, 2018], L-ODE-ODE [Rubanova *et al.*, 2019], mTAND-full.

For the interpolation task, models are trained to predict or reconstruct values for the entire dataset based on a selected subset of available points. Experiments are conducted with varying observation levels, ranging from 50% to 90% of observed points. During test time, models utilize the observed points to infer values at all time points in each test instance.

As illustrated in Table 2, MuSiCNet demonstrates superior performance, highlighting its effectiveness in time series in-

Table 1: Comparison with the baseline methods on ISMTS **classification** task.

Methods	P19		P12		PAM			
	AUROC	AUPRC	AUROC	AUPRC	Accuracy	Precision	Recall	F1 score
Transformer	80.7 \pm 3.8	42.7 \pm 7.7	83.3 \pm 0.7	47.9 \pm 3.6	83.5 \pm 1.5	84.8 \pm 1.5	86.0 \pm 1.2	85.0 \pm 1.3
Trans-mean	83.7 \pm 1.8	45.8 \pm 3.2	82.6 \pm 2.0	46.3 \pm 4.0	83.7 \pm 2.3	84.9 \pm 2.6	86.4 \pm 2.1	85.1 \pm 2.4
GRU-D	83.9 \pm 1.7	46.9 \pm 2.1	81.9 \pm 2.1	46.1 \pm 4.7	83.3 \pm 1.6	84.6 \pm 1.2	85.2 \pm 1.6	84.8 \pm 1.2
SeFT	81.2 \pm 2.3	41.9 \pm 3.1	73.9 \pm 2.5	31.1 \pm 4.1	67.1 \pm 2.2	70.0 \pm 2.4	68.2 \pm 1.5	68.5 \pm 1.8
mTAND	84.4 \pm 1.3	50.6 \pm 2.0	84.2 \pm 0.8	48.2 \pm 3.4	74.6 \pm 4.3	74.3 \pm 4.0	79.5 \pm 2.8	76.8 \pm 3.4
IP-Net	84.6 \pm 1.3	38.1 \pm 3.7	82.6 \pm 1.4	47.6 \pm 3.1	74.3 \pm 3.8	75.6 \pm 2.1	77.9 \pm 2.2	76.6 \pm 2.8
DGM ² -O	86.7 \pm 3.4	44.7 \pm 11.7	84.4 \pm 1.6	47.3 \pm 3.6	82.4 \pm 2.3	85.2 \pm 1.2	83.9 \pm 2.3	84.3 \pm 1.8
MTGNN	81.9 \pm 6.2	39.9 \pm 8.9	74.4 \pm 6.7	35.5 \pm 6.0	83.4 \pm 1.9	85.2 \pm 1.7	86.1 \pm 1.9	85.9 \pm 2.4
Raindrop	87.0 \pm 2.3	51.8 \pm 5.5	82.8 \pm 1.7	44.0 \pm 3.0	88.5 \pm 1.5	89.9 \pm 1.5	89.9 \pm 0.6	89.8 \pm 1.0
VITST	89.2 \pm 2.0	53.1 \pm 3.4	85.1 \pm 0.8	51.1 \pm 4.1	95.8 \pm 1.3	96.2 \pm 1.3	96.1 \pm 1.1	96.5 \pm 1.2
MuSiCNet	86.8 \pm 1.4	45.4 \pm 2.7	86.1 \pm 0.4	54.1 \pm 2.2	96.3 \pm 0.7	96.9 \pm 0.6	96.9 \pm 0.5	96.8 \pm 0.5

Table 2: Comparison with the baseline methods on ISMTS **interpolation** task on PhysioNet.

Observed %	50%	60%	70%	80%	90%
RNN-VAE	13.418 \pm 0.008	12.594 \pm 0.004	11.887 \pm 0.005	11.133 \pm 0.007	11.470 \pm 0.006
L-ODE-RNN	8.132 \pm 0.020	8.140 \pm 0.018	8.171 \pm 0.030	8.143 \pm 0.025	8.402 \pm 0.022
L-ODE-ODE	6.721 \pm 0.109	6.816 \pm 0.045	6.798 \pm 0.143	6.850 \pm 0.066	7.142 \pm 0.066
mTAND-Full	4.139 \pm 0.029	4.018 \pm 0.048	4.157 \pm 0.053	4.410 \pm 0.149	4.798 \pm 0.036
MuSiCNet	0.918 \pm 0.025	0.919 \pm 0.064	0.938 \pm 0.014	0.992 \pm 0.008	0.965 \pm 0.008

terpolation. This can be attributed to its ability to interpolate progressively from coarse to fine, aligning with the intuition of multi-resolution signal approximation [Mallat, 1989].

4.3 Time Series Forecasting

Datasets and Experimental Settings. (1) **USHCN** [Menne *et al.*, 2015] is an artificially preprocessing dataset containing measurements of 5 variables from 1280 weather stations in the USA. The missing ratio is 78.0%. (2) **MIMIC-III** [Johnson *et al.*, 2016] are dataset that rounded the recorded observations into 96 variables, 30-minute intervals and only use observations from the 48 hours after admission. The missing ratio is 94.2%. (3) **Physionet12** [Silva *et al.*, 2012] comprises medical records from 12,000 ICU patients. It includes measurements of 37 vital signs recorded during the first 48 hours of admission and the missing ratio is 80.4%. We use MSE to measure the forecasting performance.

Main Results of Forecasting. We compare the performance with the ISMTS forecasting models: Grafiti [Yalavarthi *et al.*, 2024], GRU-ODE-Bayes [De Brouwer *et al.*, 2019], Neural Flows [Biloš *et al.*, 2021], CRU [Schirmer *et al.*, 2022], NeuralODE-VAE [Chen *et al.*, 2018], GRUSimple, GRU-D and TLSTM [Baytas *et al.*, 2017], mTAND, and variants of Informer [Zhou *et al.*, 2021], Fedformer [Zhou *et al.*, 2022], DLinear, and NLinear [Zeng *et al.*, 2023], denoted as Informer+, Fedformer+, DLinear+, and NLinear+, respectively.

This experiment is conducted following the setting of GraFITi where for the USHCN dataset, the model observes for the first 3 years and forecasts the next 3 time steps and for other datasets, the model observes the first 36 hours in the series and predicts the next 3 time steps.

As shown in Table 3, MuSiCNet consistently achieves competitive performance across all datasets, maintaining accuracy within the top two among baseline models. While GraFITi excels by explicitly modeling the relationship between observation and prediction points, making it superior

Table 3: Experimental results for **forecasting** next three time steps. — indicates no published results.

Methods	USHCN	MIMIC-III	Physionet12
DLinear+	0.347 \pm 0.065	0.691 \pm 0.016	0.380 \pm 0.001
NLinear+	0.452 \pm 0.101	0.726 \pm 0.019	0.382 \pm 0.001
Informer+	0.320 \pm 0.047	0.512 \pm 0.064	0.347 \pm 0.001
FedFormer+	2.990 \pm 0.476	1.100 \pm 0.059	0.455 \pm 0.004
NeuralODE-VAE	0.960 \pm 0.110	0.890 \pm 0.010	—
GRU-Simple	0.750 \pm 0.120	0.820 \pm 0.050	—
GRU-D	0.530 \pm 0.060	0.790 \pm 0.060	—
T-LSTM	0.590 \pm 0.110	0.620 \pm 0.050	—
mTAND	0.300 \pm 0.038	0.540 \pm 0.036	0.315 \pm 0.002
GRU-ODE-Bayes	0.430 \pm 0.070	0.480 \pm 0.480	0.329 \pm 0.004
Neural Flow	0.414 \pm 0.102	0.490 \pm 0.004	0.326 \pm 0.004
CRU	0.290 \pm 0.060	0.592 \pm 0.049	0.379 \pm 0.003
GraFITi	0.272 \pm 0.047	0.396 \pm 0.030	0.286 \pm 0.001
MuSiCNet	0.268 \pm 0.038	0.475 \pm 0.031	0.312 \pm 0.000

Table 4: Ablation studies on different strategies of MuSiCNet in classification. \checkmark (\times) indicates the component has (not) been applied.

Component			P12	
Corr Matrix	Adjustment	Contrastive	AUROC	AUPRC
\checkmark	\checkmark	\checkmark	86.1 \pm 0.4	54.1 \pm 2.2
\times	\checkmark	\checkmark	85.5 \pm 0.3	53.0 \pm 2.1
\checkmark	\times	\checkmark	85.2 \pm 0.6	52.6 \pm 2.5
\checkmark	\times	\times	85.4 \pm 0.4	53.0 \pm 2.5
\checkmark	\checkmark	\times	85.4 \pm 0.6	52.9 \pm 2.8
\times	\times	\times	84.2 \pm 0.8	48.2 \pm 3.4

in certain scenarios, MuSiCNet remains competitive without imposing priors for any specific task.

4.4 Ablation Study

Taking P12 in the classification task as an example, we conduct the ablation study to assess the necessity of two fundamental components of MuSiCNet: correlation matrix and

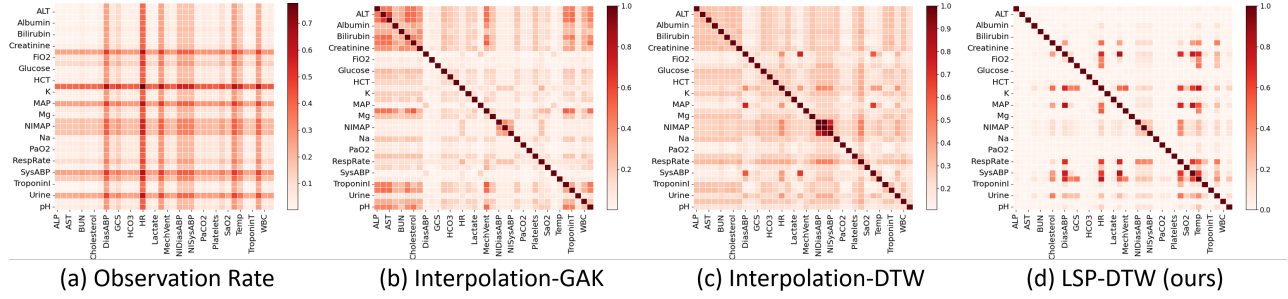


Figure 3: Visualization of various methods to extract the correlation matrix from P12 dataset. The darker the color, the more similar the relationship. (a) denotes the average pairwise observation rate (i.e., 1 minus missing rate), and (b) - (d) denotes the correlation matrices.

multi-scale learning reflected in reconstruction results adjustment and contrastive learning. As shown in Table 4, the complete MuSiCNet framework, incorporating all components, achieves the best performance. The absence of any component leads to varying degrees of performance degradation, as evidenced in layers two to five. The second layer, which retains the multi-scale learning, exhibits the second-best performance, underscoring the critical role of multi-scale learning in capturing varied temporal dependencies and enhancing feature extraction. Conversely, the version lacking all components shows a significant performance drop of 1.9%, indicating that each component is crucial to the overall effectiveness of the framework.

4.5 Correlation Results

This experiment verifies the performance of the proposed LSP-DTW and some other correlation calculation baseline methods in the P12 dataset including Interpolation-Global Alignment Kernel (I-GAK) [Cuturi, 2011], Interpolation-DTW (I-DTW) [Berndt and Clifford, 1994], and LSP-DTW. I-GAK and I-DTW are methods that interpolate the ISMTS data before computing correlations.

Interpolation for missing values significantly distorts correlation calculations, resulting in fictitious correlations in I-GAK and I-DTW matrices. I-GAK method in Fig.3(b) shows a complex pattern among variables, indicated by the darker color. Unfortunately, most correlations are negatively correlated with the observation rate, meaning pairs with lower observation rates show stronger correlations. This suggests GAK relies heavily on interpolation and may not be suitable for ISMTS data. Notably, correlations in the upper-left region appear to be artifacts of interpolation rather than actual observations. Moreover, I-DTW method in Fig.3(c) shows a relatively uniform distribution of correlations among variables. It reveals positive correlations between almost all variables, which is not intuitive and suggests I-DTW is still influenced by interpolation. In contrast, LSP-DTW accurately identifies correlations between variables, focusing on the essential characteristics of data without introducing spurious correlations from interpolation which is also verified in Table 5.

In Table 5, we keep the hyper-parameters of MuSiCNet consistent and change the correlation matrices: (1) Ones: denotes the Full-1 matrix, (2) Rand: a random symmetric matrix sampling from $[0, 1]$, (3) Diag is a diagonal-1 matrix, (4-6)

Table 5: Classification performance of MuSiCNet with different correlation matrices on P12

Corr Matrix	AUCROC	AUPRC	Corr Matrix	AUCROC	AUPRC
Ones	66.7 \pm 2.2	25.2 \pm 0.3	I-GAK	85.1 \pm 0.6	52.8 \pm 3.0
Rand	84.7 \pm 0.8	52.2 \pm 3.2	I-DTW	81.9 \pm 0.6	46.9 \pm 3.0
Diag	84.2 \pm 0.8	48.2 \pm 3.4	LSP-DTW	86.1 \pm 0.4	54.1 \pm 2.2

DTW-based methods mentioned above. We found that LSP-DTW achieved the best results, whereas I-DTW performed poorly, even worse than a random correlation matrix. This indicates that in highly sparse datasets (with a missing rate of 88.4% in P12), simple interpolation followed by similarity computation results in strong dependence on the interpolation quality, failing to capture the true correlations between variables. Ones performs significantly worse than all other methods, demonstrating that merging all input dimensions with equal weight 1 is ineffective, as it combines all variables into each channel indiscriminately. This makes Diag, which does not utilize correlations, still outperforms Ones. Other methods achieve competitive results, underscoring the importance of accurately modeling variable correlations, particularly for our LSP-DTW.

5 Conclusion

In this study, we introduce MuSiCNet, an innovative framework designed for analyzing ISMTS datasets. MuSiCNet addresses the challenges arising from data irregularities and shows superior performance in both supervised and unsupervised tasks. We recognize that irregularities in ISMTS are inherently relative and accordingly implement multi-scale learning, a vital element of our framework. In this multi-scale approach, the contribution of extra coarse-grained relatively regular series is important, providing comprehensive temporal insights that facilitate the analysis of finer-grained series. As another key component of MuSiCNet, CorrNet is engineered to aggregate temporal information effectively, employing time embeddings and correlation matrix calculating from both intra- and inter-series perspectives, in which we employ LSP-DTW to develop frequency correlation matrices that not only reduce the burden for similarity calculation for ISMT, but also significantly enhance inter-series information extraction.

6 Acknowledgments

The authors wish to thank all the donors of the original datasets and everyone who provided feedback on this work. Specially, the authors wish to thank Xiang Li and Jiaqiang Zhang for proofreading this manuscript. This work is supported by the Key Program of NSFC under Grant No.62076124 and No.62376126, Postgraduate Research & Practice Innovation Program of Jiangsu Province under Grant No.KYCX21_0225 and National Key R&D Program of China under Grant No.2022ZD0114801.

References

- [Agarwal *et al.*, 2023] Rohit Agarwal, Aman Sinha, Dilip K Prasad, Marianne Clausel, Alexander Horsch, Mathieu Constant, and Xavier Coubez. Modelling irregularly sampled time series without imputation. *arXiv preprint arXiv:2309.08698*, 2023.
- [Baytas *et al.*, 2017] Inci M Baytas, Cao Xiao, Xi Zhang, Fei Wang, Anil K Jain, and Jiayu Zhou. Patient subtyping via time-aware lstm networks. In *Proceedings of the 23rd ACM SIGKDD international conference on knowledge discovery and data mining*, pages 65–74, 2017.
- [Berndt and Clifford, 1994] Donald J Berndt and James Clifford. Using dynamic time warping to find patterns in time series. In *Proceedings of the 3rd international conference on knowledge discovery and data mining*, pages 359–370, 1994.
- [Biloš *et al.*, 2021] Marin Biloš, Johanna Sommer, Syama Sundar Rangapuram, Tim Januschowski, and Stephan Günnemann. Neural flows: Efficient alternative to neural odes. *Advances in neural information processing systems*, 34:21325–21337, 2021.
- [Cai *et al.*, 2024] Wanlin Cai, Yuxuan Liang, Xianggen Liu, Jianshuai Feng, and Yuankai Wu. Msgnet: Learning multi-scale inter-series correlations for multivariate time series forecasting. In *Proceedings of the AAAI Conference on Artificial Intelligence*, volume 38, pages 11141–11149, 2024.
- [Camino *et al.*, 2019] Ramiro D Camino, Christian A Hammerschmidt, and Radu State. Improving missing data imputation with deep generative models. *arXiv preprint arXiv:1902.10666*, 2019.
- [Che *et al.*, 2018] Zhengping Che, Sanjay Purushotham, Kyunghyun Cho, David Sontag, and Yan Liu. Recurrent neural networks for multivariate time series with missing values. *Scientific reports*, 8(1):1–12, 2018.
- [Chen *et al.*, 2018] Ricky TQ Chen, Yulia Rubanova, Jesse Bettencourt, and David K Duvenaud. Neural ordinary differential equations. *NeurIPS*, 31, 2018.
- [Chen *et al.*, 2021] Zipeng Chen, Qianli Ma, and Zhenxi Lin. Time-aware multi-scale rnns for time series modeling. In *IJCAI*, pages 2285–2291, 2021.
- [Chen *et al.*, 2022] Xinyu Chen, Chengyuan Zhang, Xi-Le Zhao, Nicolas Saunier, and Lijun Sun. Nonstationary temporal matrix factorization for multivariate time series forecasting. *arXiv preprint arXiv:2203.10651*, 2022.
- [Chowdhury *et al.*, 2023] Ranak Roy Chowdhury, Jiacheng Li, Xiyuan Zhang, Dezhi Hong, Rajesh K Gupta, and Jingbo Shang. Primenet: Pre-training for irregular multivariate time series. In *Proceedings of the AAAI Conference on Artificial Intelligence*, volume 37, pages 7184–7192, 2023.
- [Cuturi, 2011] Marco Cuturi. Fast global alignment kernels. In *Proceedings of the 28th international conference on machine learning (ICML-11)*, pages 929–936, 2011.
- [De Brouwer *et al.*, 2019] Edward De Brouwer, Jaak Simm, Adam Arany, and Yves Moreau. Gru-ode-bayes: Continuous modeling of sporadically-observed time series. *NeurIPS*, 32, 2019.
- [Du *et al.*, 2023] Wenjie Du, David Côté, and Yan Liu. Saits: Self-attention-based imputation for time series. *Expert Systems with Applications*, 219:119619, 2023.
- [Fan *et al.*, 2021] Haoqi Fan, Bo Xiong, Karttikeya Mangalam, Yanghao Li, Zhicheng Yan, Jitendra Malik, and Christoph Feichtenhofer. Multiscale vision transformers. In *Proceedings of the IEEE/CVF international conference on computer vision*, pages 6824–6835, 2021.
- [Fan, 2022] Jicong Fan. Dynamic nonlinear matrix completion for time-varying data imputation. In *AAAI*, March 2022.
- [Goldberger *et al.*, 2000] Ary L Goldberger, Luis AN Amaral, Leon Glass, Jeffrey M Hausdorff, Plamen Ch Ivanov, Roger G Mark, Joseph E Mietus, George B Moody, Chung-Kang Peng, and H Eugene Stanley. Physiobank, physiotoolkit, and physionet: components of a new research resource for complex physiologic signals. *circulation*, 101(23):e215–e220, 2000.
- [Horn *et al.*, 2020] Max Horn, Michael Moor, Christian Bock, Bastian Rieck, and Karsten Borgwardt. Set functions for time series. In *International Conference on Machine Learning*, pages 4353–4363. PMLR, 2020.
- [Jhin *et al.*, 2022] Sheo Yon Jhin, Jaehoon Lee, Minju Jo, Seungji Kook, Jinsung Jeon, Jihyeon Hyeong, Jayoung Kim, and Noseong Park. Exit: Extrapolation and interpolation-based neural controlled differential equations for time-series classification and forecasting. In *Proceedings of the ACM Web Conference 2022*, pages 3102–3112, 2022.
- [Jin *et al.*, 2022] Ming Jin, Yu Zheng, Yuan-Fang Li, Siheng Chen, Bin Yang, and Shirui Pan. Multivariate time series forecasting with dynamic graph neural odes. *IEEE Transactions on Knowledge and Data Engineering*, 2022.
- [Johnson *et al.*, 2016] AE Johnson, Tom J Pollard, Lu Shen, L-w H Lehman, Mengling Feng, Mohammad Ghassemi, Benjamin Moody, Peter Szolovits, L Anthony Celi, and Roger G Mark. Mimic-iii, a freely accessible critical care database sci. *Data*, 3(1):1, 2016.
- [Kazemi *et al.*, 2019] Seyed Mehran Kazemi, Rishab Goel, Sepehr Eghbali, Janahan Ramanan, Jaspreet Sahota, Sanjay Thakur, Stella Wu, Cathal Smyth, Pascal Poupard, and Marcus Brubaker. Time2vec: Learning a vector representation of time. *arXiv preprint arXiv:1907.05321*, 2019.

- [Kidger *et al.*, 2020] Patrick Kidger, James Morrill, James Foster, and Terry Lyons. Neural controlled differential equations for irregular time series. *NeurIPS*, 33:6696–6707, 2020.
- [Li *et al.*, 2023] Zekun Li, Shiyang Li, and Xifeng Yan. Time series as images: Vision transformer for irregularly sampled time series. In *Thirty-seventh Conference on Neural Information Processing Systems*, 2023.
- [Liu *et al.*, 2021] Shizhan Liu, Hang Yu, Cong Liao, Jianguo Li, Weiyao Lin, Alex X Liu, and Schahram Dustdar. Pyraformer: Low-complexity pyramidal attention for long-range time series modeling and forecasting. In *ICLR*, 2021.
- [Lomb, 1976] Nicholas R Lomb. Least-squares frequency analysis of unequally spaced data. *Astrophysics and space science*, 39:447–462, 1976.
- [Mallat, 1989] Stephane G Mallat. A theory for multiresolution signal decomposition: the wavelet representation. *IEEE transactions on pattern analysis and machine intelligence*, 11(7):674–693, 1989.
- [Menne *et al.*, 2015] Matthew J Menne, CN Williams Jr, and Russell S Vose. United states historical climatology network daily temperature, precipitation, and snow data. *Carbon Dioxide Information Analysis Center, Oak Ridge National Laboratory, Oak Ridge, Tennessee*, 2015.
- [Nawrot *et al.*, 2021] Piotr Nawrot, Szymon Tworkowski, Michał Tyrolski, Łukasz Kaiser, Yuhuai Wu, Christian Szegedy, and Henryk Michalewski. Hierarchical transformers are more efficient language models. *arXiv preprint arXiv:2110.13711*, 2021.
- [Neil *et al.*, 2016] Daniel Neil, Michael Pfeiffer, and Shih-Chii Liu. Phased lstm: Accelerating recurrent network training for long or event-based sequences. *NeurIPS*, 29, 2016.
- [Reiss and Stricker, 2012] Attila Reiss and Didier Stricker. Introducing a new benchmarked dataset for activity monitoring. In *2012 16th international symposium on wearable computers*, pages 108–109. IEEE, 2012.
- [Reyna *et al.*, 2020] Matthew A Reyna, Christopher S Josef, Russell Jeter, Supreeth P Shashikumar, M Brandon Westover, Shamim Nemati, Gari D Clifford, and Ashish Sharma. Early prediction of sepsis from clinical data: the physionet/computing in cardiology challenge 2019. *Critical care medicine*, 48(2):210–217, 2020.
- [Rubanova *et al.*, 2019] Yulia Rubanova, Ricky TQ Chen, and David K Duvenaud. Latent ordinary differential equations for irregularly-sampled time series. *NeurIPS*, 32, 2019.
- [Scargle, 1982] Jeffrey D Scargle. Studies in astronomical time series analysis. ii-statistical aspects of spectral analysis of unevenly spaced data. *Astrophysical Journal, Part 1, vol. 263, Dec. 15, 1982, p. 835-853.*, 263:835–853, 1982.
- [Schirmer *et al.*, 2022] Mona Schirmer, Mazin Eltayeb, Stefan Lessmann, and Maja Rudolph. Modeling irregular time series with continuous recurrent units. In *International Conference on Machine Learning*, pages 19388–19405. PMLR, 2022.
- [Shabani *et al.*, 2022] Mohammad Amin Shabani, Amir H Abdi, Lili Meng, and Tristan Sylvain. Scaleformer: Iterative multi-scale refining transformers for time series forecasting. In *The Eleventh ICLR*, 2022.
- [Shukla and Marlin, 2018] Satya Narayan Shukla and Benjamin Marlin. Interpolation-prediction networks for irregularly sampled time series. In *ICLR*, 2018.
- [Shukla and Marlin, 2020] Satya Narayan Shukla and Benjamin M Marlin. A survey on principles, models and methods for learning from irregularly sampled time series. *arXiv preprint arXiv:2012.00168*, 2020.
- [Shukla and Marlin, 2021] Satya Narayan Shukla and Benjamin Marlin. Multi-time attention networks for irregularly sampled time series. In *ICLR*, 2021.
- [Silva *et al.*, 2012] Ikaro Silva, George Moody, Daniel J Scott, Leo A Celi, and Roger G Mark. Predicting in-hospital mortality of icu patients: The physionet/computing in cardiology challenge 2012. In *2012 Computing in Cardiology*, pages 245–248. IEEE, 2012.
- [Sun *et al.*, 2021] Chenxi Sun, Shenda Hong, Moxian Song, Yen-Hsiu Chou, Yongyue Sun, Derun Cai, and Hongyan Li. Te-esn: Time encoding echo state network for prediction based on irregularly sampled time series data. In Zhi-Hua Zhou, editor, *IJCAI*, pages 3010–3016. International Joint Conferences on Artificial Intelligence Organization, 8 2021.
- [Sun *et al.*, 2024] Chenxi Sun, Hongyan Li, Moxian Song, Derun Cai, Baofeng Zhang, and Shenda Hong. Time pattern reconstruction for classification of irregularly sampled time series. *Pattern Recognition*, 147:110075, 2024.
- [Tashiro *et al.*, 2021] Yusuke Tashiro, Jiaming Song, Yang Song, and Stefano Ermon. Csd: Conditional score-based diffusion models for probabilistic time series imputation. *NeurIPS*, 34, 2021.
- [VanderPlas, 2018] Jacob T VanderPlas. Understanding the lomb–scargle periodogram. *The Astrophysical Journal Supplement Series*, 236(1):16, 2018.
- [Vaswani *et al.*, 2017] Ashish Vaswani, Noam Shazeer, Niki Parmar, Jakob Uszkoreit, Llion Jones, Aidan N Gomez, Łukasz Kaiser, and Illia Polosukhin. Attention is all you need. *NeurIPS*, 30, 2017.
- [Villani and others, 2009] Cédric Villani et al. *Optimal transport: old and new*, volume 338. Springer, 2009.
- [Wang *et al.*, 2024] Jun Wang, Wenjie Du, Wei Cao, Keli Zhang, Wenjia Wang, Yuxuan Liang, and Qingsong Wen. Deep learning for multivariate time series imputation: A survey. *arXiv preprint arXiv:2402.04059*, 2024.
- [Wu *et al.*, 2020] Zonghan Wu, Shirui Pan, Guodong Long, Jing Jiang, Xiaojun Chang, and Chengqi Zhang. Connecting the dots: Multivariate time series forecasting with graph neural networks. In *Proceedings of the 26th ACM*

- SIGKDD international conference on knowledge discovery & data mining*, pages 753–763, 2020.
- [Wu *et al.*, 2021] Yinjun Wu, Jingchao Ni, Wei Cheng, Bo Zong, Dongjin Song, Zhengzhang Chen, Yanchi Liu, Xuchao Zhang, Haifeng Chen, and Susan B Davidson. Dynamic gaussian mixture based deep generative model for robust forecasting on sparse multivariate time series. In *AAAI*, volume 35, pages 651–659, 2021.
- [Yalavarthi *et al.*, 2024] Vijaya Krishna Yalavarthi, Kiran Madhusudhanan, Randolph Scholz, Nourhan Ahmed, Johannes Burchert, Shayan Jawed, Stefan Born, and Lars Schmidt-Thieme. Grafiti: Graphs for forecasting irregularly sampled time series. In *Proceedings of the AAAI Conference on Artificial Intelligence (AAAI)*, pages 16255–16263, 2024.
- [Yoon *et al.*, 2018] Jinsung Yoon, James Jordon, and Michaela Schaar. Gain: Missing data imputation using generative adversarial nets. In *International conference on machine learning*, pages 5689–5698. PMLR, 2018.
- [Yu *et al.*, 2024] Zhihao Yu, Xu Chu, Liantao Ma, Yasha Wang, and Wenwu Zhu. Imputation with inter-series information from prototypes for irregular sampled time series. *arXiv preprint arXiv:2401.07249*, 2024.
- [Zeng *et al.*, 2023] Ailing Zeng, Muxi Chen, Lei Zhang, and Qiang Xu. Are transformers effective for time series forecasting? In *Proceedings of the AAAI conference on artificial intelligence*, volume 37, pages 11121–11128, 2023.
- [Zhang *et al.*, 2021a] Pengchuan Zhang, Xiyang Dai, Jianwei Yang, Bin Xiao, Lu Yuan, Lei Zhang, and Jianfeng Gao. Multi-scale vision longformer: A new vision transformer for high-resolution image encoding. In *Proceedings of the IEEE/CVF international conference on computer vision*, pages 2998–3008, 2021.
- [Zhang *et al.*, 2021b] Xiang Zhang, Marko Zeman, Theodoros Tsiligkaridis, and Marinka Zitnik. Graph-guided network for irregularly sampled multivariate time series. In *ICLR*, 2021.
- [Zhang *et al.*, 2021c] Zhao-Yu Zhang, Shao-Qun Zhang, Yuan Jiang, and Zhi-Hua Zhou. Life: Learning individual features for multivariate time series prediction with missing values. In *2021 IEEE International Conference on Data Mining (ICDM)*, pages 1511–1516. IEEE, 2021.
- [Zhao *et al.*, 2021] Yucheng Zhao, Chong Luo, Zheng-Jun Zha, and Wenjun Zeng. Multi-scale group transformer for long sequence modeling in speech separation. In *IJCAI*, pages 3251–3257, 2021.
- [Zhou *et al.*, 2021] Haoyi Zhou, Shanghang Zhang, Jieqi Peng, Shuai Zhang, Jianxin Li, Hui Xiong, and Wancai Zhang. Informer: Beyond efficient transformer for long sequence time-series forecasting. In *Proceedings of the AAAI conference on artificial intelligence*, volume 35, pages 11106–11115, 2021.
- [Zhou *et al.*, 2022] Tian Zhou, Ziqing Ma, Qingsong Wen, Xue Wang, Liang Sun, and Rong Jin. Fedformer: Frequency enhanced decomposed transformer for long-term series forecasting. In *International conference on machine learning*, pages 27268–27286. PMLR, 2022.

A Pseudo Code for MuSiCNet

The Pseudo Code is provided using classification as an example. The interpolation task can be obtained by removing the projection head f_{cls} and the classification loss term \mathcal{L}_{cls} from the total loss in line #17. While in the case of forecasting tasks, the projection head will be replaced with f_{fore} and task loss will be changed to $\mathcal{L}_{\text{fore}}$ as in Eq.11.

Algorithm 1 MuSiCNet Algorithm for Classification

Input: Training set \mathcal{X} , the number of scale layers L , random masking ratio r , max reference point number $|\tau^{(L)}|$, hyper-parameters $\lambda_1, \lambda_2, \lambda_3$.

Parameters: Encoder model f_{CorrE} , decoder model f_{CorrD} , GRU model f_{GRU} , projection head f_{cls}

Output: Encoder model f_{CorrE} , GRU model f_{GRU} , projection head f_{cls}

```

1:  $C_T \leftarrow \text{Eq.}(2)$  with  $\mathcal{X}$ 
2: for  $\mathbf{X}$  in  $\mathcal{X}$  do
3:    $\{\mathbf{X}^{(1)}, \dots, \mathbf{X}^{(L)}\} \leftarrow \text{Mask}_r(\text{AvgPooling}_L(\mathbf{X}))$ 
4:    $\ell_{\text{recon}} \leftarrow 0$ 
5:   for  $l \leftarrow 1$  to  $L$  do
6:      $\mathbf{r}^{(l)} \leftarrow f_{\text{CorrE}}(\mathbf{X}^{(L)}, C_T, |\tau^{(L)}|/2^{(L-l)})$ 
7:      $\mathbf{h}^{(l)} \leftarrow f_{\text{GRU}}(\mathbf{r}^{(l)})$ 
8:      $\hat{\mathbf{X}}_{\text{recon}}^{(l)} \leftarrow f_{\text{CorrD}}(\mathbf{r}^{(l)}, |\mathbf{X}^{(l)}|)$ 
9:      $\ell_{\text{recon}} \leftarrow \ell_{\text{recon}} + \text{Eq.}(3)$  with  $\mathbf{X}^{(l)}$  and  $\hat{\mathbf{X}}^{(l)}$ 
10:   end for
11:    $\ell_{\text{adj}}, \ell_{\text{cons}} \leftarrow 0, 0$ 
12:   for  $l \leftarrow 2$  to  $L$  do
13:      $\ell_{\text{adj}} \leftarrow \ell_{\text{adj}} + \text{Eq.}(5)$  with  $\hat{\mathbf{X}}^{(l-1)}$  and  $\hat{\mathbf{X}}^{(l)}$ 
14:      $\ell_{\text{cons}} \leftarrow \ell_{\text{cons}} + \text{Eq.}(6)$  with  $\mathbf{h}^{(l-1)}$  and  $\mathbf{h}^{(l)}$ 
15:   end for
16:    $\mathcal{L}_{\text{cls}} \leftarrow \text{Eq.}(9)$  with  $\mathbf{h}^{(L)}$ 
17:    $\mathcal{L}_{\text{overall}} \leftarrow \frac{1}{L}\ell_{\text{recon}} + \frac{\lambda_1}{L-1}\ell_{\text{adj}} + \frac{\lambda_2}{L-1}\ell_{\text{cons}} + \lambda_3\mathcal{L}_{\text{cls}}$ 
18:   Update overall network parameters
19: end for
```

B Time Embedding in CorrNet

Time Embedding method embeds continuous time points of ISMTS into a vector space [Kazemi *et al.*, 2019; Shukla and Marlin, 2021]. It leverages H embedding functions $\phi_h(t)$ simultaneously and each outputting a representation of size d_r . Dimension i of embedding h is defined as follows:

$$\phi_h(t)[i] = \begin{cases} \omega_{0h} \cdot t + \alpha_{0h}, & \text{if } i = 0 \\ \sin(\omega_{ih} \cdot t + \alpha_{ih}), & \text{if } 0 < i < d_r \end{cases} \quad (7)$$

where the ω_{ih} 's and α_{ih} 's are learnable parameters that represent the frequency and phase of the sine function. This time embedding method can capture both non-periodic and periodic patterns with linear and periodic terms, respectively.

C ISMTS Analysis Tasks

The overall loss is defined as Eq.(8), incorporating an optional task-specific loss component.

$$\mathcal{L} = \sum_{l=1}^L \ell_{\text{recon}}^{(l)} + \lambda_1 \ell_{\text{adj}}^{(l)} + \lambda_2 \ell_{\text{cons}}^{(l)} \quad (8)$$

Supervised Learning. We augment the encoder-decoder CorrNet by integrating a supervised learning component that utilizes the latent representations for feature extraction. In this work, we specifically concentrate on classification tasks as a representative example of supervised learning. The loss function is

$$\mathcal{L}_{\text{cls}} = \frac{1}{C} \sum_{c=1}^C \frac{1}{n^c} \sum_{i=1}^{n^c} \ell_{CE}(\text{CLS}(\mathbf{h}_i^{(L)}), y_i) \quad (9)$$

where C denotes the number of classes, n^c denotes the number of samples in c -th class, $\text{CLS}(\cdot)$ denotes the projection head for classification, and $\ell_{CE}(\cdot)$ denotes the cross-entropy loss.

Unsupervised Learning. For our unsupervised learning example, we choose interpolation and forecasting. The loss function for interpolation is defined as

$$\mathcal{L}_{\text{int}} = \sum_i \|\mathbf{M}^{(L)} \odot ((\hat{\mathbf{X}}_{\text{reco}}^{(L)})_i - \mathbf{X}_i^{(L)})\|_2^2 \quad (10)$$

This equation essentially represents the reconstruction outcome at the finest scale as $\ell_{\text{adj}}^{(L)}$ in Eq.(4) making the interpolation task fit seamlessly into our model with minimal modifications. Therefore, it is unnecessary to incorporate an additional loss function into our overall loss function Eq.(8).

While the loss function for forecasting is defined as

$$\mathcal{L}_{\text{fore}} = \sum_i \|(\mathbf{M}_{\text{fore}})_i \odot ((\hat{\mathbf{X}}_{\text{fore}}^{(L)})_i - (\mathbf{X}_{\text{fore}})_i)\|_2^2 \quad (11)$$

As observations might be missing also in the groundtruth data, to measure forecasting accuracy we average an element-wise loss function $\mathcal{L}_{\text{fore}}$ over only valid values using $(\mathbf{M}_{\text{fore}})_i$.

D Further Details on Datasets

We adopt the data processing approach used in RAINDROP [Zhang *et al.*, 2021b] for the classification task, mTANs [Shukla and Marlin, 2021] for the interpolation task, and GraFITi [Yalavarthi *et al.*, 2024] for the forecasting task. The aforementioned processing methods serve as the usual setup, which our method also follows for fair comparison. *However, it's important to note that we do not incorporate static attribute vectors* (such as age, gender, time from hospital to ICU admission, ICU type, and length of stay in ICU) in our processing. This decision is based on the fact that our model, MuSiCNet, is not specifically designed for clinical datasets. Instead, it is designed as a versatile, general model capable of handling various types of datasets, which may not always include such static vectors. The detailed information of base-lines is in Table 6.

D.1 Datasets for Classification

P19: PhysioNet Sepsis Early Prediction Challenge 2019. P19 dataset [Reyna *et al.*, 2020] comprises data from 38, 803 patients, each monitored by 34 irregularly sampled sensors, including 8 vital signs and 26 laboratory values. The original dataset contained 40, 336 patients, but we excluded those

Table 6: Statistics of the ISMITS datasets used in our experiments. “#Avg. obs.” denotes the average number of observations for each sample.

Tasks	Datasets	#Samples	#Variables	#Avg. obs.	#Classes	Imbalanced	Missing ratio
Classification	P19	38,803	34	401	2	True	94.9%
	P12	11,988	36	233	2	True	88.4%
	PAM	5,333	17	4,048	8	False	60.0%
Interpolation	PhysioNet	4,000	37	2,880	-	-	78.0%
Forecasting	USHCN	1,100	5	263	-	-	77.9%
	MIMIC-III	21,000	96	274	-	-	94.2%
	Physionet12	5,333	37	130	-	-	85.7%

with excessively short or long time series, resulting in a range of 1 to 60 observations per patient as in RAINDROP. Each patient has a binary label representing the occurrence of sepsis within the next 6 hours. The dataset has a high imbalance with approximately $\sim 4\%$ positive samples.

P12: PhysioNet Mortality Prediction Challenge 2012. P12 [Goldberger *et al.*, 2000] includes data from 11,988 patients after removing inappropriate 12 samples as explained in [Horn *et al.*, 2020]. This dataset features multivariate time series from 36 sensors collected during the first 48 hours of ICU stay. Each patient has a binary label indicating the length of stay in the ICU, in which a negative label for stays under 3 days and a positive label for longer stays. P12 is imbalanced with $\sim 93\%$ positive samples.

PAM: PAMAP2 Physical Activity Monitoring. PAM [Reiss and Stricker, 2012] records the daily activities of 9 subjects using 3 inertial measurement units. RAINDROP has adapted it for irregularly sampled time series classification by excluding the ninth subject for short sensor data length. The continuous signals were segmented into samples with the window size 600 and 50% overlapping rate. Originally with 18 activities, we retain 8 with over 500 samples each, while others are dropped. After modification, PAM includes 5,333 sensory signal segments, each with 600 observations from 17 sensors at 100 Hz. To simulate irregularity, 60% of observations are randomly removed by RAINDROP, uniformly across all experimental setups for fair comparison. The 8 classes of PAM represent different daily activities, with no static attributes and roughly balanced distribution.

D.2 Dataset for Interpolation

Physionet: PhysioNet Challenge 2012 dataset Physionet [Reiss and Stricker, 2012] comprises 37 variables from ICU patient records, with each record containing data from the first 48 hours after admission to ICU. Aligning with the methodology of Neural ODE [Rubanova *et al.*, 2019], we round observation times to the nearest minute, resulting in up to 2,880 potential measurement times for each time series. The dataset encompasses 4,000 labeled instances and an equal number of unlabeled instances. For our study, we utilize all 8,000 instances in interpolation experiments. Our primary objective is to predict in-hospital mortality, with 13.8% of the instances belonging to the positive class.

D.3 Dataset for Forecasting

USHCN: U.S. Historical Climatology Network. USHCN [Menne *et al.*, 2015] data are used to quantify national and

regional-scale temperature changes in the contiguous United States. It contains measurements of 5 variables from 1280 weather stations. Following the preprocessing proposed by [De Brouwer *et al.*, 2019], the majority of the over 150 years of observations are excluded, and only data from the years 1996 to 2000 are used in the experiments. Furthermore, to create a sparse dataset, only a randomly sampled 5% of the measurements are retained.

Physionet12. This dataset consists of medical records from 12,000 ICU patients. During the first 48 hours of admission, measurements of 37 vital signs were recorded. Following the forecasting approach used in recent work, such as [Yalavarthi *et al.*, 2024; Biloš *et al.*, 2021; De Brouwer *et al.*, 2019], we pre-process the dataset to create hourly observations, resulting in a maximum of 48 observations per series.

MIMIC-III: Medical Information Mart for Intensive Care. MIMIC-III [Johnson *et al.*, 2016] is a widely utilized medical dataset offering valuable insights into ICU patient care. To capture a diverse range of patient characteristics and medical conditions, 96 variables are meticulously observed and documented. For consistency, we followed the preprocessing steps outlined in previous studies [Yalavarthi *et al.*, 2024; Schirmer *et al.*, 2022; Biloš *et al.*, 2021; De Brouwer *et al.*, 2019]. Specifically, we rounded the recorded observations to 30-minute intervals and used only the data from the first 48 hours post-admission. Patients who spent less than 48 hours in the ICU were excluded from the analysis.

E Experimental details

E.1 MuSiCNet parameters

We present the training hyperparameters and model parameters here. The maximum epoch is set to 300, and AdamW optimizer is selected as our optimizer without weight decay. By default, the learning rate is set to $1e-3$, and the learning rate schedule is cosine decay for each epoch. Batch size for all datasets is set to 50, the dimension of the encoder output is set to 256, and the dimension of the hidden representations in GRU is typically set to 50. The random masking ratio r for each scale is set to 0.1.

Due to inconsistent series lengths, we set the maximum reference point number to 128 for long series, such as P12, PAM, PhysioNet and USHCN, to 96 for Physionet12, and to 48 for short series, such as PAM and MIMIC-III.

Initially, the window size is set to $1/4$ of the time series length and then halved iteratively until the majority of the

windows contain at least one observation.

According to the observed timestamps on each dataset, the number of scale layers L is set to 6, 5, 7, 6, 8, 4, and 5 for P12, P19, PAM, Physionet, USHCN, MIMIC-III, and Physionet12, respectively. For example, in classification, for P12, the scales are 4, 8, 16, 32, 64 and raw length. For P19, the scales are 4, 8, 16, 32 and raw length. And for PAM, the scales are 4, 8, 16, 32, 64, 128 and raw length. In all mainstream tasks involved, the hyperparameters $\lambda_1, \lambda_2, \lambda_3$ are selected in $[1e-3, 1e-2, \dots, 1e2]$. All the models were experimented using the PyTorch library on a GeForce RTX-2080 Ti GPU.

E.2 Baseline Parameters

The implementation of baseline models adheres closely to the methodologies outlined in their respective papers, including SeFT [Horn *et al.*, 2020], GRU-D [Che *et al.*, 2018], mTAND [Shukla and Marlin, 2021] and ViTST [Li *et al.*, 2023]. We follow the settings of the attention embedding module baseline in mTAND and implement the Multi-Correlation Attention module in our work.